

# Measuring Residual Stresses in Orthotropic Steel Decks Using the Incremental Hole-Drilling Technique

W. Nagy<sup>1</sup>  · E. Van Puymbroeck<sup>1</sup> · K. Schotte<sup>1</sup> · P. Van Bogaert<sup>1</sup> · H. De Backer<sup>1</sup>

Received: 6 September 2016 / Accepted: 13 January 2017 / Published online: 23 January 2017  
© The Society for Experimental Mechanics, Inc 2017

**Abstract** Manufacturing processes such as welding cause residual stresses which exist in most steel civil structures, causing plastic deformations without any external loads. This type of stress is often overlooked during design. Nevertheless, residual stresses can have serious influence on the material strength and the fatigue life of the construction. This is also true for orthotropic steel decks which have many complex welding details. Since little is known about the distribution of residual stresses due to welding, a semi-destructive experimental test setup is developed for a stiffener-to-deck plate connection of an orthotropic steel deck. In particular, hole-drilling is used. The test procedure has been optimized to reduce measurement errors. The most important influencing factors on measurement accuracy are the surface preparation and the precision of the determination of the zero-depth. Once these measurement errors are optimized using proper grinding and visual inspection tools, a clear residual stress pattern becomes visible. The results confirmed the theoretical assumption of high tensile yield stresses near the weld location.

However, at small distance from the weld, the residual stresses tend to decrease to almost zero.

**Keywords** Orthotropic steel deck · Hole-drilling · Residual stress · Fatigue · Strain gauge rosette

## Introduction

Residual stresses are introduced unintentionally by almost every manufacturing process, such as rolling, forming, milling, welding, etc. Sometimes they are even intentionally introduced by the use of a surface treatment such as shot-peening in order to compensate for other types of residual stresses. The effect of residual stress can be either beneficial or detrimental, depending on the magnitude, sign and distribution of the introduced stresses. The presence of tensile residual stress is especially harmful due to its contribution to fatigue failure. The opposite is true for compressive residual stresses being present [1–3]. They are usually beneficial as they increase wear and corrosion resistance and prevent the initiation and propagation of fatigue cracks [4]. Due to the fact that residual stress creates plastic deformations without any external load, it is ignored when evaluating fatigue failure using Eurocode 3 [5], because the stress variations only are considered. A possible solution for this omission is the use of Linear Elastic Fracture Mechanics (LEFM). This fatigue assessment method allows adding an initial stress state to the stress variations due to an external load [2]. However, in most cases more research concerning the actual magnitude and distribution of the residual stresses in steel structures is needed.

This is especially true for Orthotropic Steel Decks (OSDs) which suffer from important fatigue problems due to the extensive use of welded connections (Fig. 1). These bridge decks consist of a grillage of closed trapezoidal longitudinal

---

✉ W. Nagy  
Wim.Nagy@UGent.be

E. Van Puymbroeck  
Evy.VanPuymbroeck@UGent.be

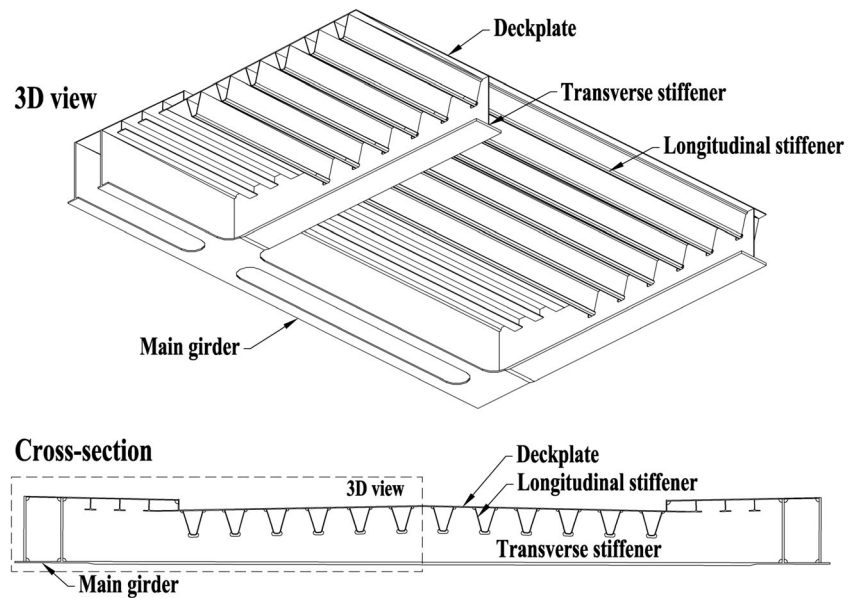
K. Schotte  
Ken.Schotte@UGent.be

P. Van Bogaert  
Philippe.VanBogaert@UGent.be

H. De Backer  
Hans.DeBacker@UGent.be

<sup>1</sup> Ghent University – Department of Civil Engineering, Technologiepark 904, B-9052 Zwijnaarde, Belgium

**Fig. 1** Cross-section and 3D view of an orthotropic steel deck



stiffeners and transverse webs welded to a deck plate. They are widely used in long span bridges since they are extremely light weighted when compared to their load carrying capacity and are therefore durable and very efficient. Since the introduction of orthotropic steel decks, several fatigue problems at welding details have been observed. Some examples are: the Moerdijk Bridge in the Netherlands, Severn Crossing in the United Kingdom and the Haseltal and Sinntal viaducts in Germany [6, 7]. The increased traffic intensity and individual traffic loads when compared to design load assumptions are the main reasons for this phenomenon. In addition, recently constructed bridges such as the Temse bridge in Belgium (1994) and the Van Brienoord bridge in the Netherlands (1990) have developed fatigue cracks [8, 9]. This indicates a lack of knowledge concerning the fatigue behaviour in these decks. The unknown residual stress distribution and its influence on the fatigue lifetime is especially important. Based on the experience of an OSD with open stiffeners, tensile yield stresses are expected for closed stiffeners in the area around the weld and compressive stresses outside this area with a magnitude of 25 % of the yield stress [10]. At present, this assumption is often used for the fatigue evaluation of OSDs with closed stiffeners [11, 12].

### Incremental Hole-Drilling Technique

Various methods have been developed to measure residual stresses for different types of components. The three main categories for classifying residual stress measurements are: destructive, semi-destructive and non-destructive measuring techniques. Both the destructive and the semi-destructive techniques depend on determining the residual stress from

the deformation caused by completely or partially relieving the residual stress through material removal [4]. These deformations are determined during or after the test procedure. Splitting, sectioning, Incremental Hole-Drilling (IHD), ring-core and deep core are some of the main techniques that are based on the (semi-)destructive stress relaxation method. Although these techniques are very straightforward, they are not recommended or even possible to use as an inspection tool. Non-destructive techniques can therefore offer a solution. These techniques, such as X-ray diffraction [13], ultrasonic and magnetic methods [14] can be used to evaluate the residual stresses in, for example, bridges or aerospace structures. The principle of non-destructive techniques is based on measuring a parameter that is related to the residual stress distribution without damaging the specimen. However, with these techniques, often a material-specific calibration is needed on test pieces without any residual stresses. Therefore, the reliability of these methods relies on the performed calibration.

A widely used process for measuring residual stresses in materials is the IHD technique. The main advantage of this method is the semi-destructive character: it relies on drilling a small hole into the specimen which causes only limited damage that is often tolerable or easy to repair. In addition, this method is convenient to use, has standard procedures and has a good accuracy and reliability [15].

### Principle of IHD Measuring

The IHD technique involves drilling a small blind hole into the test material at the location where the residual stresses are to be evaluated. This implies that the hole is not drilled through the thickness of the test material. The removal of the

material results in a redistribution of the residual stress field in the material surrounding the hole and localized deformations in the test specimen. Using special Strain Gauge Rosettes (SGRs), the relieve of the surface strains is measured simultaneously at incremental depths. The holes are drilled through the centre of these strain gauge rosettes. The corresponding strains from the drilling process can then be evaluated at each depth with the standardized test procedure described in ASTM E837-13a [16]. Using this test procedure and based on knowledge of literature about the practical application [17] and on the measurement accuracy [18], a proper precision and reliability of the residual stress calculation can be obtained. Figure 2 illustrates the positioning of the drilling cutter on the SGR and the deformation because of the hole drilling when assuming tensile residual stresses within the material. Due to the relaxation of the tensile residual stresses, the hole tends to expand horizontally with a small vertical surface rise due to the Poisson effect [15]. The opposite behaviour is found for the case of compressive residual stresses.

### IHD Test Setup

To determine the residual stress distribution close to a welded stiffener-to-deck plate connection of an OSD, a full scale test specimen has been constructed with dimensions comparable with current OSD designs (Fig. 3). This bridge deck is 8.2 m long and 4.1 m wide. The deck plate is supported by three crossbeams and two main girders. Therefore, the deck plate consists out of two spans of 4.1 m each. The main girders are simply supported at the crossbeam locations which results in a configuration of six supports in total. Figure 3b illustrates the cross section of the OSD test specimen. The closed longitudinal trapezoidal stiffeners are 300 mm high, 300 mm wide at the top and 125 mm at the lower soffit. The deck plate has 15 mm thickness while the stiffeners have 6 mm thickness. Additionally, steel quality S235 is used. This implies that a yield strength of 235 MPa is used, combined with a young

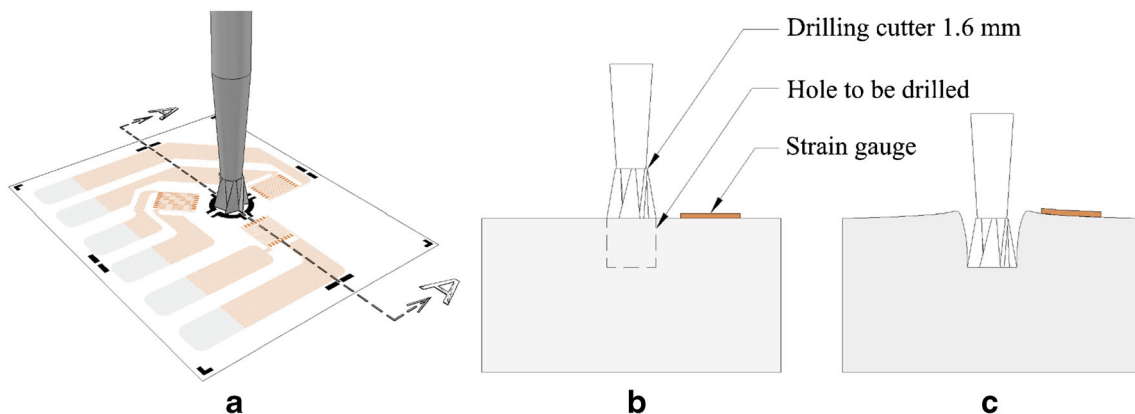


**Fig. 2** Schematic overview of the hole-drilling technique. (a) Strain gauge rosette and drilling cutter of 1.6 mm; (b) cross-section A-A before drilling; (c) cross-section A-A after drilling

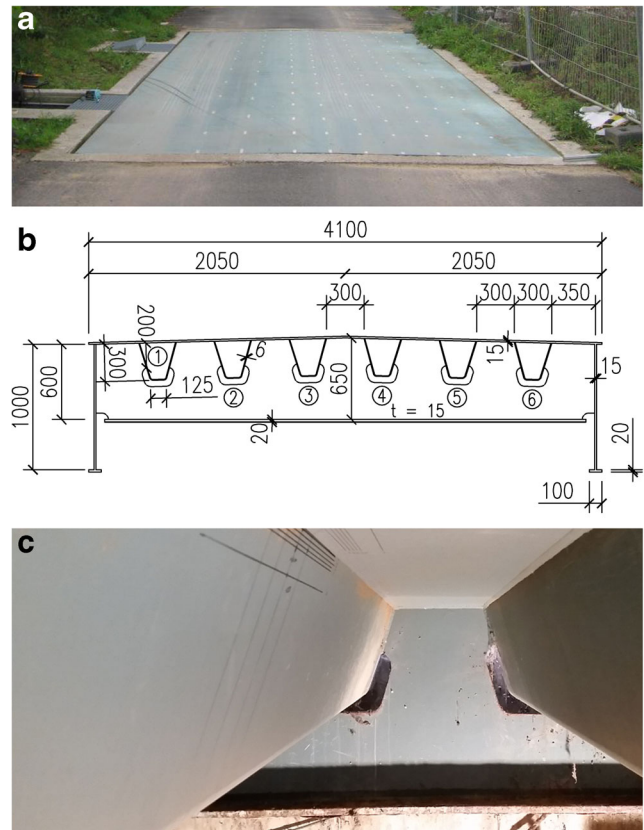


**Fig. 3** Full scale test specimen of an OSD. (a) Top view of the steel deck; (b) Cross-section of the OSD; (c) Bottom view between two longitudinal stiffeners

modulus of 210 GPa. Furthermore, the connecting welds have an approximate throat thickness of 4 mm. Finally, no asphalt layer is added on the deck plate. A relative thick layer of paint is used instead to protect the OSD against corrosion.

Figure 4 indicates the cross-section of the chosen grid pattern for installing the different SGRs. This cross-section is placed in the middle of the first span of the OSD and at the second longitudinal stiffener. The SGRs are placed on the top and bottom of the deck plate and at the exterior of the

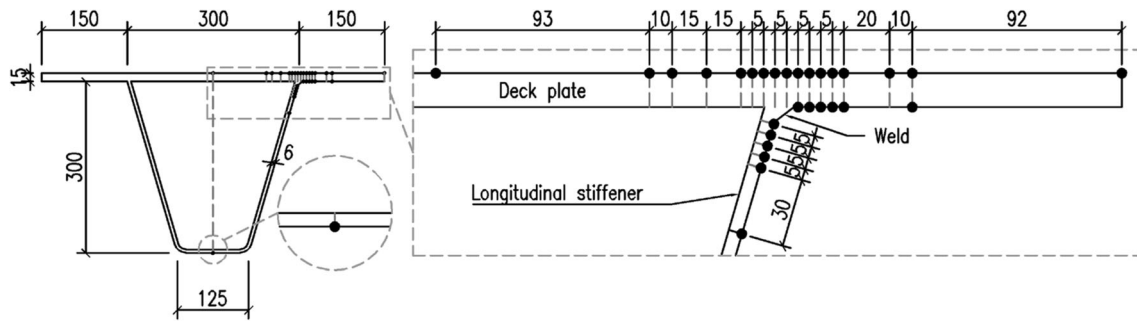


**Fig. 4** Cross-section of the hole-drilling locations and indication of the measuring points

longitudinal stiffener in the vicinity of the weld region. There are no measuring points at the inside of the stiffener because the hole drilling rig has to be perpendicular to the SGRs this being impossible at the inside of the stiffener.

A total of 59 SGRs, two different type A SGRs and one type B SGRs, were used for the whole test setup. Both the type A and B rosettes consist of three radial strain gauges measuring strains in longitudinal and transversal direction as well as at a  $45^\circ$  angle. With these strains, the three in-plane stresses  $\sigma_x$ ,  $\sigma_y$  and  $\tau_{xy}$  can be evaluated using the IHD technique calibration matrix from the ASTM E837-13a [16]. To measure strains adjacent to the weld toe, type B strain gauges rosettes (CEA-06-062UM-120 [19]) are used. The arrangement of all three measurement grids at the same side of the hole allows for drilling as close as possible to the weld toe (Fig. 5(b)). However, this configuration increases the sensitivity to eccentricity errors of the hole and is therefore only used for the positions adjacent to the weld toe. All other IHD technique positions are equipped with type A SGRs (CEA-06-062UL-120 [19]) with a maximum hole diameter of 2 mm (Fig. 5(a)). With these types of SGRs, the three radial strain gauges are divided around the circumference of the drill centre. According to the standardized ASTM [16], these SGRs are applicable for non-distributive stress calculations up to a depth of 1 mm. Thus, nine larger SGRs are used at critical points to evaluate the residual stresses at larger depth, up to 2 mm. These SGRs are also of the type A (CEA-06-125RE-120 [19]), but allow a maximum hole diameter of 4.1 mm (Fig. 5(c)). Due to the increase of the hole diameter and larger deformation, residual stress evaluation at larger depths becomes possible.

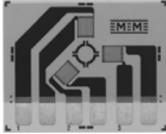
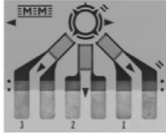

Finally, the SGR spacing has to be considered. The relaxation effects of drilling a hole at the centre of a SGR extend beyond the boundaries of the rosette. According to literature [16, 17, 20], the minimum distance between two adjacent holes should be at least six times the hole diameter. The relaxation effect at larger distance is limited to less than 1 %. For this reason, not all strain gauges from Fig. 4 are placed in the same cross-section of the OSD. In total nine cross-sections with a spacing of 50 mm are used to distribute all the different SGRs so the previous recommendation is valid for all measuring points. The use of different cross-sections is justified as the relevant residual stresses are those perpendicular to the weld direction. The residual stresses do not vary considerably in the longitudinal direction as the weld quality due to the fully automated welding procedure should be quite the same along the entire length of the weld. In addition, the distribution of the nine cross-sections only enclose a weld length of 450 mm compared to the full weld length of 4100 mm. Therefore, the considered cross-sections may still be considered as being at the span centre of the OSD and thus no interference of the crossbeams should be present.

A final remark concerns the strain gauge grid. The latter is chosen to match both with the top deck plate grid and its bottom deck counterpart. SGRs on both sides of the deck plate, show identical locations, which increases the comparability of all the measured residual stresses.

**Surface preparation of the test specimen** According to the instruction Bulletin B-129-8 [21] for proper installation of a SGR, the surface preparation before applying a strain gauge

**Fig. 5** Used strain gauges for the test procedure. (a) Type B strain gauge for applications close to welds or obstacles; (b) Type A strain gauge for a drilled depth up to 1 mm; (c) Type A strain gauge for a drilled depth up to 2 mm

Strain gauge rosette  
Matrix dimension (L x W)  
Grid center diameter  
Strain gauge length  
Resistance

	a	b	c
Strain gauge rosette			
CEA-06-062UL-120	CEA-06-062UM-120	CEA-06-125RE-120	
Matrix dimension (L x W)	12.7 x 15.7 mm	9.6 x 12.2 mm	19.8 x 19.8 mm
Grid center diameter	5.13 mm	5.13 mm	10.26 mm
Strain gauge length	1.57 mm	1.57 mm	3.18 mm
Resistance	120 $\Omega$	120 $\Omega$	120 $\Omega$

has to include the following steps: solvent degreasing, abrading, marking the gauge layout lines, conditioning the surface and finally neutralizing the surface. Especially for the IHD method, the second and third steps are of major importance as they can influence the strain results. In the particular case of an OSD with a relatively thick layer of paint, mechanical grinding was necessary. Special care is needed with mechanical grinding to ensure that no additional residual stresses are created. The magnitude of these potential additional residual stresses can be reduced when the grinding speed is at maximum and the heat dispersion is as low as possible.

Initially, an angle grinder with an abrasive mop disc was used with a grit size of 80 (Fig. 6(a), top) for the first 27 strain gauges. The angle grinder has a fixed speed of 8500 rpm. This type of grinding results in very smooth surface preparation (Fig. 6(a), bottom). In addition, manual wet grinding was used with abrasive paper with a grit size of 400 and a mild phosphoric-acid compound. After the surface abrading, the SGR layout lines have to be marked on the surface. This has to be as precise as possible to reduce the misalignment errors in further calculations. The reference lines should be marked with tools that burnish rather than scratch the surface. This could be done with a drafting pencil or a round-pointed ball-point pen [21]. The latter has been chosen as this resulted in the most visible layout lines. After marking the layout lines, the contact surface should be degreased and pH-neutralized using an effective degreasing solvent, water-based acid and

alkaline surface cleaners. This surface preparation protocol results in a clean and smooth surface for optimal strain gauge bond and improves the accuracy of the strain results.

Although a smooth surface could be accomplished with an abrasive mop disc, this may be too aggressive when looking at the near-surface stresses as a thin steel layer is removed. In addition, the drawing of the gauge layout lines could also influence the near surface stresses as they could create small additional residual stresses. To compare this first surface preparation process, both the technique of abrading and marking the gauge layout lines has been changed for the remaining 32 SGRs. Alternatives for removing the paint layer with an angle grinder are for example a knotted wire cup brush (Fig. 6(b), top) or a crimped wire cup brush (Fig. 6(c), top). The results of these grinding techniques are visualised in the bottom of Fig. 6(b) and (c), respectively. As the knotted wire cup brush was the least aggressive, not all impurities could be removed between the grains (Fig. 6(b), bottom). In addition, the surface is not really sufficiently smooth for gluing the strain gauges to the surface. Therefore, the crimped wire cup brush was used for the remaining SGRs. As illustrated in the bottom of Fig. 6(c), the surface is almost polished without removing any steel. Compared to the knotted wire, it is somewhat more aggressive, and it also flattens the surface grains. As with the abrasive mop disc, manual wet grinding was applied after the mechanical grinding. Immediately after abrading the surface, the contact surface was degreased and pH-neutralized using

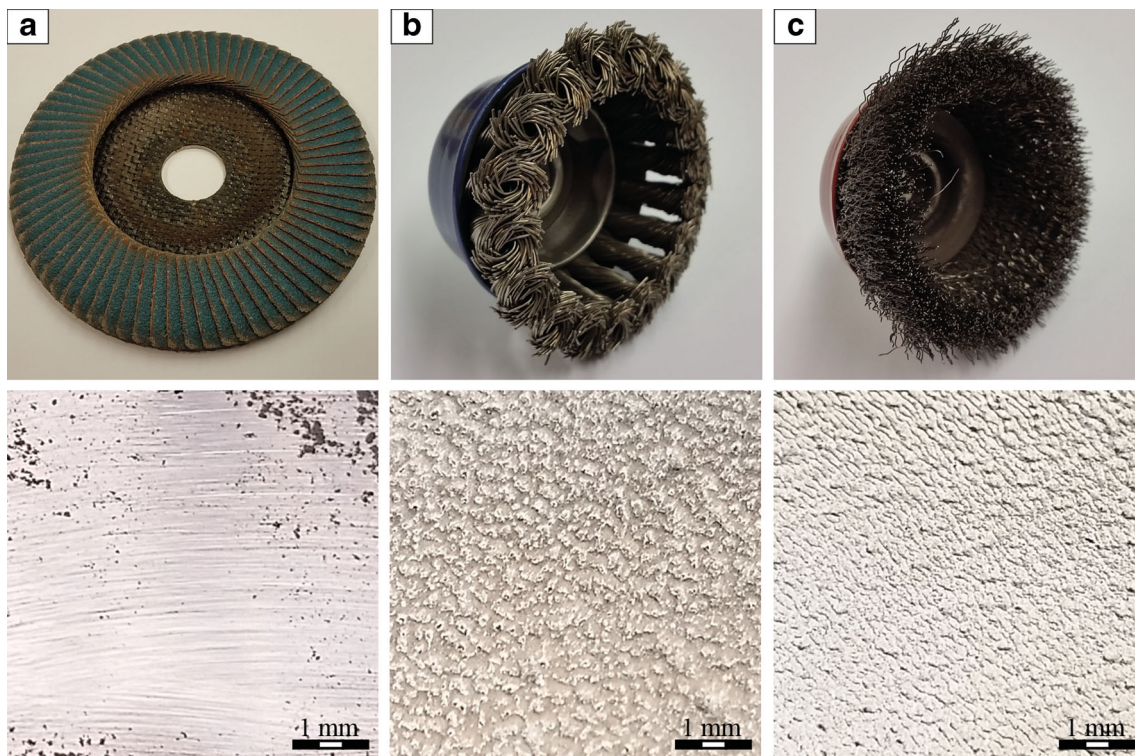


**Fig. 6** Used abrading technique with an angle grinder and their influence on the prepared surface. (a) Abrasive mop disc; (b) Knotted wire cup brush; (c) Crimped wire cup brush

an effective degreasing solvent and water-based acid and alkaline surface cleaners. The gauge layout lines are marked after this procedure, only in an area around the SGRs, never below the actual surface of the strain gauges. Again, this is done with a round-pointed ballpoint pen without really burrishing the surface. This implies that the influence of the residual stresses due to the reference lines should be minimized. However, the measurement error due to misalignment of the SGRs increases slightly. To reduce this possible error, every strain gauge alignment was checked by virtually extending the gauge layout lines with a 20 cm ruler and if necessary corrected before bonding.

**Practical guidelines for installing the strain gauges and the data-acquisition system** The SGRs used for the IHD technique contain three quarter bridge strain gauge grids each. The carrier and protection layer of the strain gauge grids consists of a thin polyimide layer, while the measuring grid is a self-temperature-compensated constantan foil. The thermal expansion coefficient of  $10.8 \cdot 10^{-6} / \text{K}$  matches the temperature response of the OSD steel. The resistance of the strain gauges is  $120 \Omega$ . The bonding of the SGRs is done using a fast-drying, easily applicable and creep-free cyanoacrylate glue.

Although all SGRs contain solder taps on which the lead wires can be connected, the use of additional soldering islands is chosen. This allows the connection to be independent from the carrier in order to provide strain relief for the strain gauge connections as the lead wires could tear the strain gauge during soldering. The independent soldering islands are connected to the strain gauges with a thin insulated solid copper wire. This connection is created with a loose loop in the wire to ensure no strains can occur during soldering.

Depending on the data acquisition system, a three-wire or four-wire Wheatstone bridge completion can be used. In this case, a four-wire configuration is applied. Compared to the three-wire configuration, the four-wire has the advantage of directly compensating the lead wire resistance during measurement. The resistance of the lead wires could change during measurement if the wires are accidentally pulled or experience heat transfer from an external source. As a result of using a four-wire bridge completion, these external effects have no influence on the measurements and the strain accuracy is assured.

Finally, the used soldering flux in the solder to prevent oxidation during soldering is removed by using a rosin solvent to prevent degradation of the protective coatings, corrosion of the metals and to eliminate conductive flux residues. Afterwards, a nitrile rubber protective coating is applied on the SGR, soldering islands and all non-insulated connections and wires. Therefore, all sensitive elements are protected during drilling and since this acts as an insulator, the steel particles from the drilling process cannot cause any electrical interference with the soldered connections.

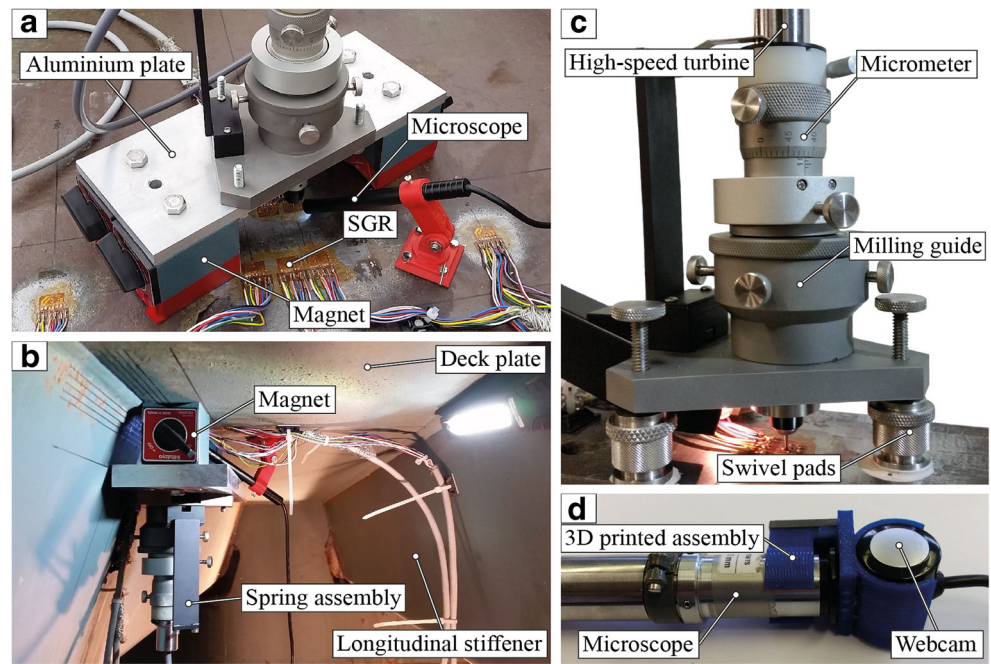
During the IHD procedure, the strains are continuously measured with a high precision data acquisition system, allowing for an accuracy of  $\pm 1 \mu\text{S}$  (microstrain) or less. Furthermore, the strains used for the IHD procedure are based on the smoothed data of the measured strains with a frequency of 10 Hz. More precisely, the smoothed data represents the moving average of the last ten measured strains. By doing this, random noise is reduced.

**Setup of the milling guide** A special milling guide is needed to execute the IHD process. It has to allow a very precise positioning above the centre of the SGRs and has to be perfectly perpendicular to the surface. The RS-200 milling guide allows for this precision [22]. Normally, the milling guide is attached to the test specimen using three levelling screws, each equipped with a swivelling mounting pad which can be attached to uneven surfaces (Fig. 7(c)). This setup has been modified to increase the time efficiently and to be able to drill as close as possible to the weld toe without being obstructed by the longitudinal stiffener. This includes using powerful V-prism magnets, inducing an attractive vertical force of 900 N connected to the milling guide using a 10 mm thick aluminium plate (Fig. 7(a) and (b)). Depending on the position, up to four magnets can be used. Due to the welding procedure used for OSDs, the deck plate and stiffener will have some global deformations. These deformations will however never affect the planarity of the local surface below the milling guide. Therefore, assuming a flat surface of the test specimen, the milling guide will always be perfectly perpendicular to the surface and it is very easy in use, not depending on the fast-setting-cement kit which is traditionally used for attaching the swivelling mounting pads.

After global positioning of the milling guide, it is centred more precisely over the SGR and a high-speed air turbine is inserted, equipped with a carbide, inverted cone, dental bur with a diameter of 1.6 mm.

Before the milling procedure is started, zero calibration of the strain gauge is needed. This zero calibration has to correspond to zero depth of the milling guide. This zero depth is reached by cutting through the backing material of the strain gauge and barely scratching the surface of the test specimen. This has to be done very carefully because the error on the zero-depth will highly influence the strain/stress results at larger depths. To optimize this, the milling process is simultaneously monitored with a USB-powered microscope with a magnification of 200x (Figs. 7(a) and 8). The chance of missing the zero-depth is therefore minimized. In addition, the strain measurements are carefully monitored to notice any changes in the strains. When the strain values are already changed at zero-depth, too much material has already been removed from the test specimen and an error on the zero-depth is present.

**Fig. 7** Milling guide setup. (a) Milling guide attached to the top deck plate; (b) Milling guide attached underneath the deck plate; (c) Standard milling guide setup (d) Modified microscope with an additional webcam



Finally, when zero-depth has been reached, the holes are incrementally drilled until the final depth corresponding to the used SGR. In total, three different drill sequences were used. The first one is a constant step sequence of  $76.2\ \mu\text{m}$  steps up to a final depth of  $1828.8\ \mu\text{m}$ . The other sequences are increased with depth. For a drilled depth of 1 mm, the following sequence is used: 3 steps of  $25.4\ \mu\text{m}$  followed by 23 steps of  $76.2\ \mu\text{m}$ . For a drilled depth of 2 mm, the sequence is: 4 steps of  $25.4\ \mu\text{m}$ , followed by 2 steps of  $50.8\ \mu\text{m}$  and 20 steps of  $101.6\ \mu\text{m}$ . After the final depth has been reached, the final hole diameter is measured with the same microscope as for positioning the milling guide. This was not possible for the SGRs at the longitudinal stiffener because there was insufficient space between the microscope and the next longitudinal stiffener for the

observer. Therefore, a modification is made for these particular cases. An adapter has been developed with a 3D-printer to fit a webcam to the eyepiece of the microscope (Fig. 7(d)). As a result, the microscope readings can still be done using a laptop and therefore the milling guide can be used in tight spaces.

**The orbital drilling technique** When using the milling guide RS-200, only inverted carbide burs with a diameter of  $1.6\ \text{mm}$  are available. If a larger diameter is necessary, orbital drilling becomes necessary (Fig. 8). This is achieved by giving the bur a radial offset relative to the axial centreline of the turbine assembly. In addition, drilling using the maximum prescribed SGR diameter is advised as this results in larger strain results and therefore in more accurate results in depth. Furthermore,

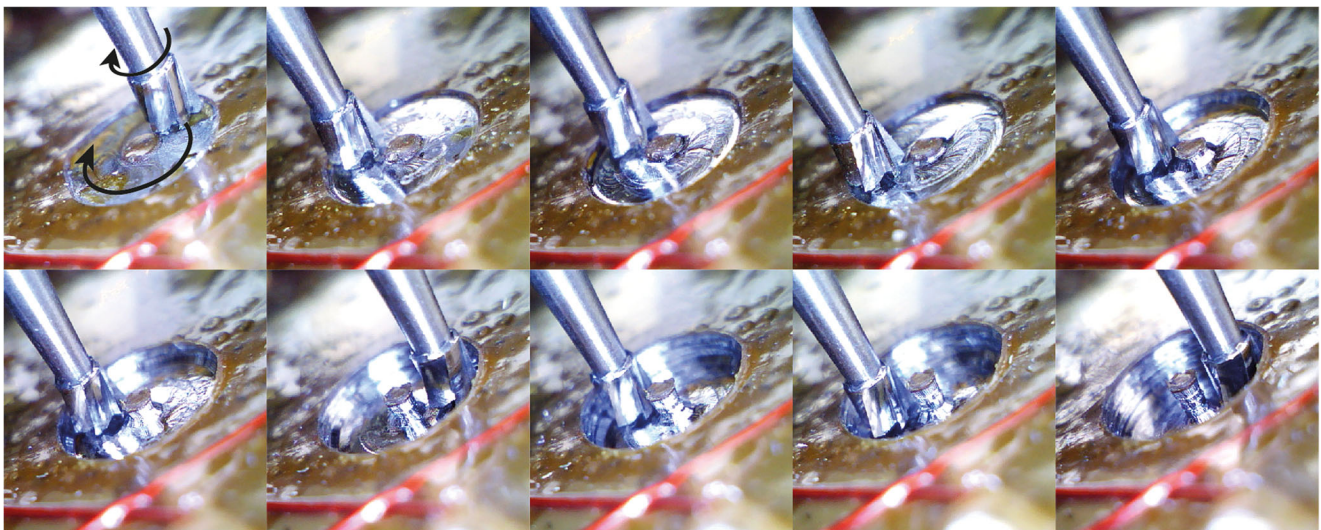


**Fig. 8** Incremental orbital drilling of a large SRG with a hole diameter of 4 mm

the use of orbital drilling strongly diminishes the effect of the chamfer, present on the inverted carbide burs, resulting in a perfectly drilled, cylindrical hole. The latter is necessary as the used calibration matrix presented by ASTM E837-13a [16], determined using the finite element method, assumes a perfectly cylindrical shape for the hole [23]. For these reasons, the smallest SGRs are drilled with a hole diameter of 2 mm and the large ones with a hole diameter of 4 mm. Due to the limited bur size, a small stub remains at the inside of the drilled hole with a diameter of 4 mm (Fig. 8). This however does not influence the measurements as the redistribution of the residual stresses and the localized deformations at the border of the drilled hole are not interrupted by this small stub.

## Experimental Procedure

The determination of the non-uniform residual stresses is done using the H-Drill [24] program, which is based on ASTM E837-13a [16]. The measured strains and corresponding depths are imported in the program and smoothed based on the Tikhonov regularization. This is needed to reduce the errors in the calculated stresses as the magnitude of small strain fluctuations with depth are magnified into unrealistic stress fluctuations. Using a set of standard calibration matrices, the residual stresses can be evaluated at every measured depth.

## Results

### Determining the Non-uniform Stresses

Figure 9(b) and (c) illustrate the variation of the non-uniform residual stresses with the depth for the first 27 SGRs which are installed using an abrasive mop disc as surface preparation. These curves are all for SGRs on the top of the deck of the OSD test specimen. It can be noted that a large range of near-surface stresses are present, varying from yield compressive residual stresses of  $-235$  MPa and higher up to tensile residual stresses of 125 MPa. At larger depth, most of the residual stress curves decrease until a stable value is reached at final depth. The large scatter of the near-surface stresses can be due to the used abrading technique. When using an abrasive mop disc, a small amount of steel will be removed which results in a measurement error of the actual drilled depth. In addition, when looking to Fig. 6(a), the abrading technique used creates some scratches on the surface with a certain directionality. Therefore, the possible surface stresses due to the abrading technique depend on the orientation of the scratched compared to the installed SGR. Consequently, these potential stresses vary for all SGRs as the grinding orientation is arbitrary.

Another remark concerns the burnishing of the reference lines, as this can also influence the results. During burnishing,

minimal local plastic deformation occurred since after polishing with the ballpoint pen a shallow curvature within the deck plate remained visible. This implies that the used pressure on the ballpoint pen was sufficient to achieve the local yield strength. Therefore, it is possible that the burnishing operation increased the compressive stress near the surface.

As the initial values of the near-surface strains influence the calculation of the stress results at final depth, the method of adding reference lines has been changed in the last 5 SGRs of the first installed 27 strain gauges (Fig. 9(c)). A round-pointed ballpoint pen has been used with decreased pressure on the surface and at a distance of 0.5 mm from the SGR. Hence, no reference lines appear below the SGRs. The influence of using an abrasive mop disc, but changing the technique of adding reference lines is illustrated in Fig. 9(c). All near-surface stresses are varying between  $-101$  and 125 MPa. In addition, these curves tend to vary little and result in almost uniform stresses. Based on these results compared to Fig. 9(b), the use of a ballpoint pen has a serious influence on the near-surface stresses up to a depth of 0.5 mm. At larger depth, both the abrading technique and the added reference lines do not seem to influence the residual stresses [17].

When changing the abrading technique as described in paragraph “Surface preparation of the test specimen” and not using reference lines below the SGRs, the measured residual stress curves all have a similar trend and the near-surface stresses are closer in range (Fig. 9(d)). Only one curve (black) is off-scale, but this is due to a missed zero-depth. These curves illustrate the increased accuracy when using a proper abrading technique and adding layout lines outside the region of the strain gauges. The reason why high compressive near-surface residual stresses are measured is not clear. Either the abrading technique still introduces additional residual stresses or these stresses are present due to the manufacturing process (e.g. rolling). Nevertheless, this only influences a very thin surface layer.

### Effect of Drilling Sequence on Stress Determination Accuracy

The accuracy of the strain results decreases with the hole depth as the material removal is located away from the SGR. Therefore, a small error in the strain results at larger depth results in a larger error in the stress calculation. In addition, due to the coupling in the calculation method and the effect of the quality of the experimental data, the sensitivity within depth could increase and oscillation about the original stress level is most likely present. Based on literature [17, 25, 26], this sensitivity to strain errors can be reduced if a proper calculation sequence is used. An optimized distribution of the depth increments has been proposed depending on the relevant depth of the stress measurement. If the stress at larger



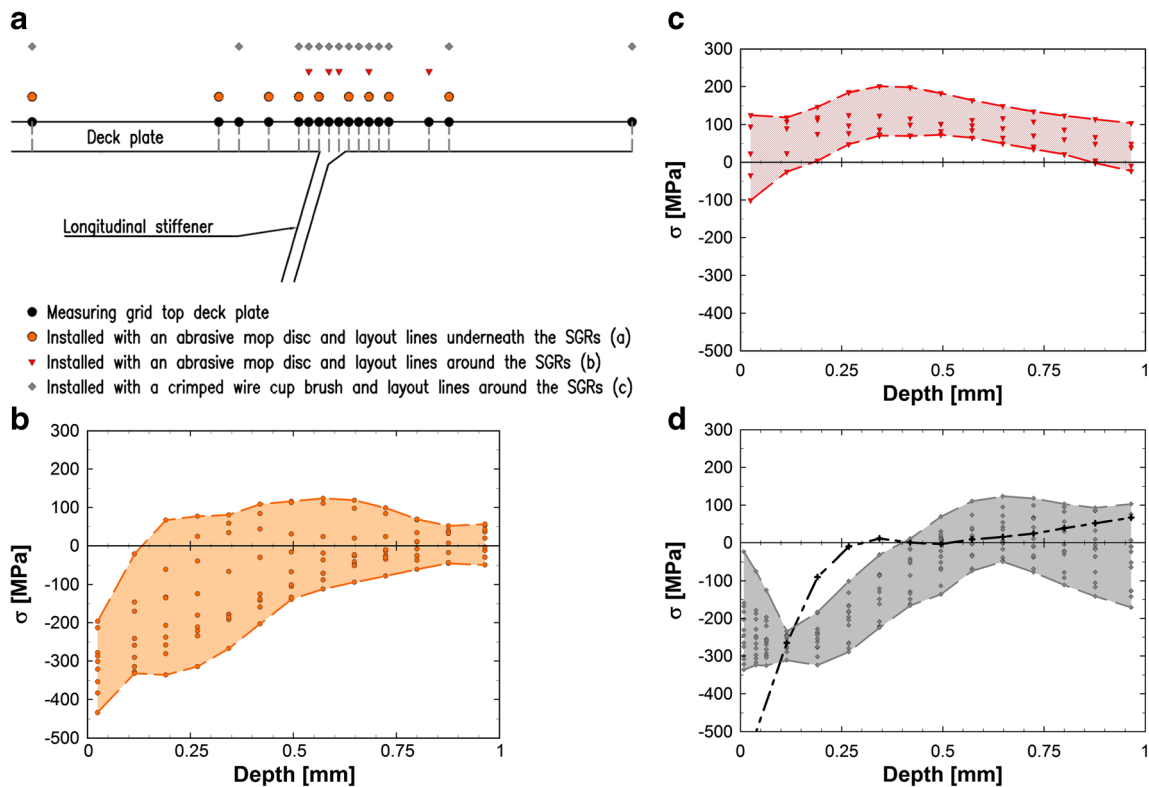


**Fig. 9** Comparison of the non-uniform stresses using different surface preparations. **(a)** Location of the installed SGRs; **(b)** Non-uniform stresses determined using an abrasive mop disc and a constant step sequence of 76.2  $\mu\text{m}$ ; **(c)** Non-uniform stresses determined using an

abrasive mop disc and a constant step sequence of 76.2  $\mu\text{m}$ ; **(d)** Non-uniform stresses determined using a crimped wire brush and an increased step sequence: 3 steps of 25.4  $\mu\text{m}$  followed by steps of 76.2  $\mu\text{m}$

depth is to be determined, the proposed drill sequence uses a constant depth increment of 128  $\mu\text{m}$ . Subsequently, the stresses are calculated using five calculation increments: 2 increments of 128  $\mu\text{m}$ , 2 increments of 256  $\mu\text{m}$  followed by a 512  $\mu\text{m}$  increment. If near-surface stresses are important, both the drill sequence and the calculation increments should be: 4 increments of 32  $\mu\text{m}$ , 4 increments of 64  $\mu\text{m}$  followed by 8 increments of 128  $\mu\text{m}$ . Obviously, using less steps to measure the stresses at larger depth, results in loss of detail in the measured stresses. Hence, a comparison has to be made between the accuracy of measured stress versus the magnitude of the possible errors.

The sequence for the first 27 SGRs consists of a constant incremental step of 76.2  $\mu\text{m}$  up to a final depth of 1828.8  $\mu\text{m}$ . The remaining 32 SGRs are drilled with a modified sequence using incremental steps. The reason for the modification after the first 27 SGRs is to investigate the influence of the calculation sequence on the accuracy, as well as to increase the accuracy on the detection of the zero-depth. Due to the amount of reflection on the microscope image, it could happen to misinterpret the zero-depth. To reduce this uncertainty, the incremental steps at the beginning are kept at the minimal step size of 25.4  $\mu\text{m}$ . Once the strain results confirmed a change in the measured strains, the previous data point and depth is accepted as the real zero-depth. Following the zero-depth

determination, the sequence up to a final depth of 1828.8  $\mu\text{m}$  for both the CEA-06-062UM-120 and the CEA-06-062UL-120 SGRs is: 3 steps of 25.4  $\mu\text{m}$ , followed by 23 steps of 76.2  $\mu\text{m}$ . The larger SGRs (CEA-06-125RE-120) use the following sequence up to a final depth of 2235.2  $\mu\text{m}$ : 4 steps of 25.4  $\mu\text{m}$ , followed by 2 steps of 50.8  $\mu\text{m}$  and 20 steps of 101.6  $\mu\text{m}$ .

Figure 9(d) illustrates the influence of using a proper incremental sequence. More data points become available near the surface compared to the stresses calculated based on a constant depth sequence in Fig. 9(b) and (c). The black curve in Fig. 9(d) also demonstrates the effect of missing the correct zero-depth in the measurements.

Figure 10(a) and (b) clarify the influence of the calculation sequence. As for the majority of the SGRs, strain results were very smooth and showed limited variation with depth. Therefore, the calculated stresses regarding the used sequence are very accurate. Figure 10(a) is such an example. Compared to the original curve with the same calculation sequence as the drill sequence, three other calculation sequences are plotted: S1 = 24 steps of 76.2  $\mu\text{m}$ ; S2 = 12 steps of 152  $\mu\text{m}$ ; S3 = 6 steps of 76.2  $\mu\text{m}$ , followed by 9 steps of 152  $\mu\text{m}$ . The coarser sequences mainly have an influence on the near-surface stress calculations, but the overall stress curve is almost identical. Therefore, it can be concluded that the drill sequence has no

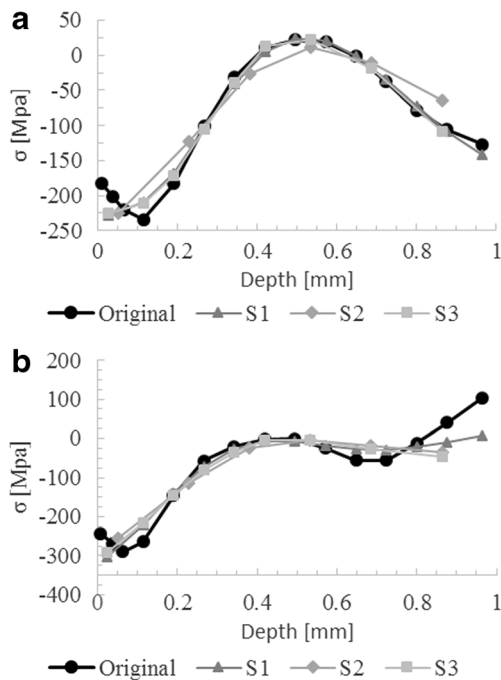


**Fig. 10** Influence of the used drilled sequence on the accuracy. (a) SGR with a high accuracy of strain readings; (b) SGR with small strain fluctuations

real influence on the final depth stresses if the strain results are of high quality. Figure 10(b) on the other hand is an example where the error on the strain results at larger depth is somewhat higher. A small error at larger depth automatically results in large stress variations. In this case, using a coarser sequence results in a smoother and more stable curve. This is mainly due to the used integration method as the sensitivity of the near-surface strains will influence the sensitivity of the strains at larger depth. When increasing the size of the steps in the calculation sequence, fewer data points are available and the smoothing based on the Tikhonov regularization will result in a smoother curve. This smoothing by using a coarser calculation sequence is allowed only when the strain results indicate some strain errors fluctuating with depth. If the strain changes in depth are obviously not due to some measurement errors, the smoothing is not advisable as this will result in a lack of accuracy in the real non-uniform stress pattern.

### Orbital Drilling

Some of the results of the larger SGRs are illustrated in Fig. 11. Figure 11(a) and (b) clearly indicate that the measured stresses at larger depth (125RE) are almost identical to those measured using the smaller SGRs (062UL), assuming the latter already indicate a constant stress value at final depth. However, the near-surface stresses are not very accurate as these types of strain gauges are not really suited for this [17]. Most importantly, if the stresses at a depth of 1 mm are still not converging, as shown in Fig. 11(c), the larger SGRs

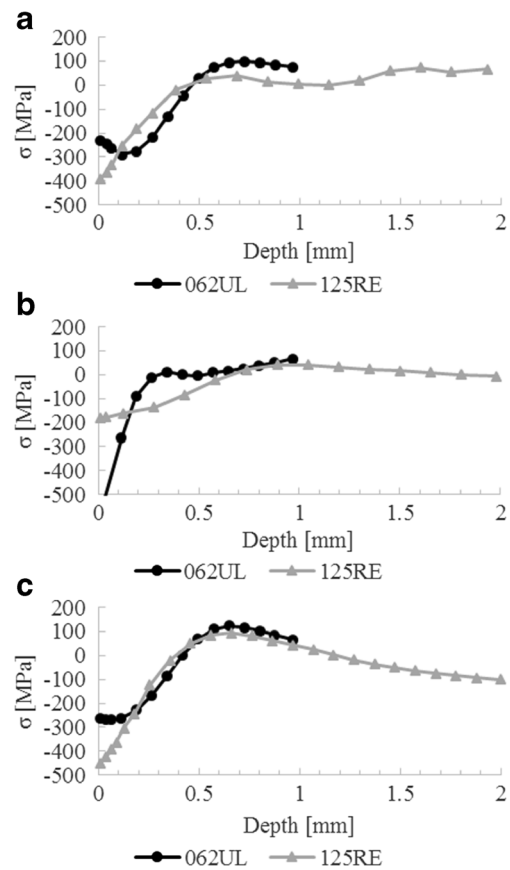


**Fig. 11** Comparison of using small SRGs to large SRGs

provide more information at larger depth, where the residual stresses might already converge. Still, when considering the amount of time needed to drill the larger SGRs (see Table 1), these should only be applied when the residual stresses at 1 mm are still not converging.

### Stress Distribution Pattern

Figure 12 summarize the residual stress in the transversal direction. In addition, the shown residual stresses are grouped depending on the used surface preparation. Table 1 clarifies this surface preparation and indicates the displayed stress depth. As the IHD technique is only applicable in the linear elastic region, stresses higher than the yield strength are topped-off at the yield strength of 235 MPa. The near-surface stresses (G3) practically equal the yield strength as was already shown in Fig. 9. At the final depth of 1 mm, it can be noted that residual stresses up to tensile yield strength are indeed present near the weld toe. On top of the deck plate, compensating residual compressive stresses are found. This is also confirmed by the larger SGRs (G5) at a final depth of 2 mm. Although the deck plate is 15 mm thick, an acceptable residual stress distribution can be found by using only SGRs for a depth up to 1 mm. Larger SGRs are necessary at those locations where the residual stresses are still not converging at

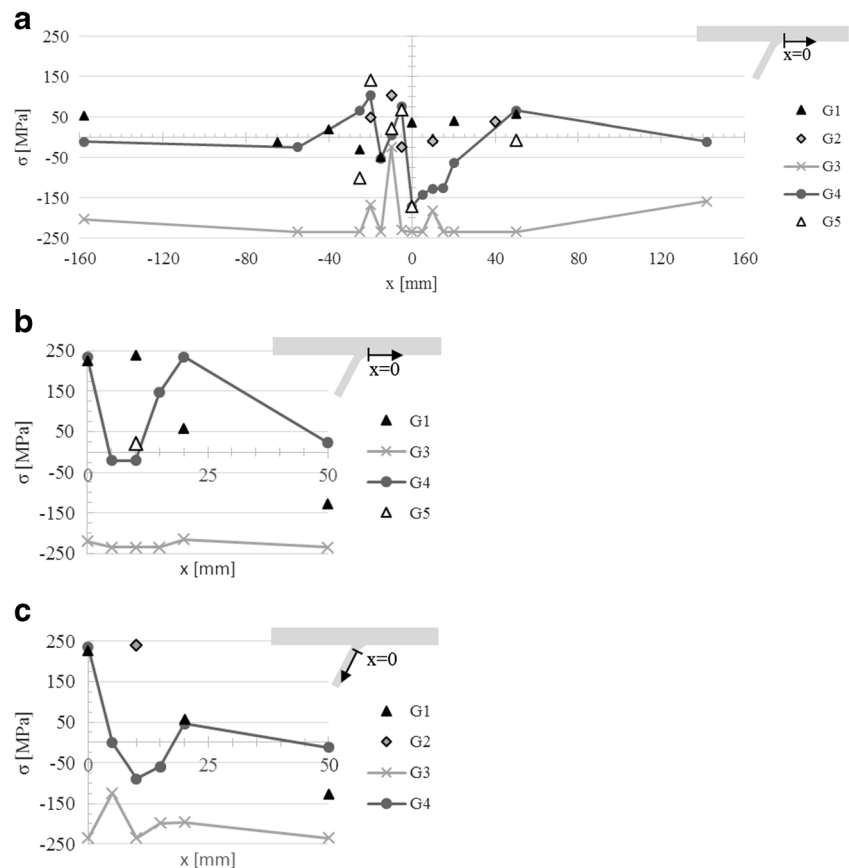
**Table 1** Used surface preparation corresponding with the SGR group

	Group of strain gauge rosettes				
	G1	G2	G3	G4	G5
Used strain gauge rosettes					
CEA-06-062UL-120	✓	✓	✓	✓	
CEA-06-062UM-120	✓		✓	✓	
CEA-06-125RE-120					✓
Applied technique					
Abrasive mop disc	✓	✓			
Crimped wire cup brush			✓	✓	✓
Layout line underneath the SGR	✓				
Layout lines surrounding the SGR		✓	✓	✓	✓
Drill parameters					
Average hole diameter [mm]	1.939	1.951	1.947	1.947	4.058
Std. hole diameter [mm]	0.053	0.032	0.050	0.050	0.157
Total drilled depth [mm]	1.829	1.829	1.829	1.829	2.235
Average drill time [min]	39	39	39	39	81
Evaluated stress depth [mm]	<b>0.965</b>	<b>0.965</b>	<b>0.008</b>	<b>0.965</b>	<b>0.965</b>

depth of 1 mm, which is only the case at one location. All other strain gauges of this type confirm the earlier results. At one location a shift occurred since at 1 mm depth the residual stresses had a tensile sign, whereas at 2 mm depth, the sign

was inverted with a similar magnitude of stresses. The SRGs of groups G1 and G2 are not taken into account for the final distribution of the residual stresses as they have too many uncertainties due to the used surface preparation technique

**Fig. 12** Overview of the measured residual stresses on all measuring points. (a) Top deck plate; (b) Bottom deck plate; (c) Longitudinal stiffener



and the less accurate zero depth determination. This is translated in more scatter and often a too large shift compared to the results from SGR groups G4 and G5.

At further distance from the weld region, the residual stresses decrease until very low compressive stresses are found of about 5 % of the yield strength. This is much lower than the assumption of 25 % which can be found in the literature [10].

## Conclusions

Using the IHD technique as an assessment tool for determining residual stresses has many benefits. Due to its semi-destructive character, the existing residual stresses become visible without really damaging the test specimen. In addition, as it is a very sensitive analysing tool, several guidelines and recommendations have to be taken into account. First of all, the surface preparation before bonding the SRG can have a high influence on the measured stresses, especially if the near-surface stresses are of interest. It is advised to avoid mechanical grinding as much as possible. If mechanical grinding is inevitable, a crimped wire cub brush in combination with high grinding speed results in a smooth surface with no or a very thin effect of additional residual stresses. Furthermore, the determination of the zero-depth is of high importance. To eliminate a misinterpreted zero-depth, a combination of a live microscopic image and an adjusted minimum drilling depth and continuous measuring of strains should be used.

When assessing the calculated residual stresses, it can be concluded that the used drill sequence can have an impact on the reliability of the near-surface stresses or the stresses at final depth. The accuracy of both can be achieved if the measurement of strains is of high quality. In addition, if the residual stresses are still not converged at a final depth of 1 mm, it is advisable to use larger SGRs as they could complete the residual stress pattern.

In conclusion, the IHD technique allows obtaining a clear pattern of existing residual stresses near welded locations without really damaging the structure. This knowledge can highly improve future fatigue calculations, which is especially necessary for OSDs.

## References

- Acevedo C, Nussbaumer A (2012) Effect of tensile residual stresses on fatigue crack growth and S-N curves in tubular joints loaded in compression. *Int J Fatigue* 36:171–180
- Barsoum Z, Barsoum I (2009) Residual stress effects on fatigue life of welded structures using LEFM. *Eng Fail Anal* 16:449–467
- Torres MAS, Voorwald HJC (2002) An evaluation of shot peening, residual stress and stress relaxation on the fatigue life of AISI 4340 steel. *Int J Fatigue* 24:877–886
- Rossini NS, Dassisti M, Benyounis KY et al (2012) Methods of measuring residual stresses in components. *Mater Des* 35:572–588
- CEN/TC 250 (2005) EN 1993-1-9:2005/AC:2009 - Design of steel structures - Part 1-9: Fatigue 34
- de Jong FBP (2004) Overview fatigue phenomenon in orthotropic bridge decks in the Netherlands. In: 2004 Orthotropic Bridge Conference. ASCE, Sacramento, p 489–512
- Wolchuk R (1990) Lessons from weld cracks in orthotropic decks on three European bridges. *J Struct Eng* 116:75–84
- Maljaars J, van Dooren F, Kolstein H (2012) Fatigue assessment for deck plates in orthotropic bridge decks. *Steel Constr* 5:93–100
- Nagy W, Diversi M, van Bogaert P et al (2014) Improved fatigue assessment techniques of connecting. In: Eurosteel 2014. Naples, Italy, p 1–8
- Connor R, Fisher J, Gatti W et al (2012) Manual for design, construction, and maintenance of orthotropic steel deck bridges. US Department of Transportation, Federal Highway Administration
- Xiao ZG, Yamada K, Inoue J et al (2006) Fatigue cracks in longitudinal ribs of steel orthotropic deck. *Int J Fatigue* 28:409–416
- Bignonnet A, Carracilli J, Jacob B (1991) ÉTUDE en FATIGUE des PONTS MÉTALLIQUES par un MODÈLE de MÉCANIQUE de la RUPTURE. *Ann l'Institut Tech du bâtiment des Trav publics* 493:57–96
- Xu L, Zhang S-Y, Sun W et al (2015) Residual stress distribution in a Ti-6Al-4V T-joint weld measured using synchrotron X-ray diffraction. *J Strain Anal Eng Des* 50:445–454
- Santa-aho S, Sorsa A, Nurmikolu A et al (2014) Review of railway track applications of Barkhausen noise and other magnetic testing methods. *Insight* 56:657–663
- Schajer GS (2013) Practical residual stress measurement methods. John Wiley & Sons Ltd, United Kingdom
- ASTM International. Determining residual stresses by the hole-drilling strain-gage method. ASTM E837-13a 2013; 1–16
- Grant PV, Lord JD, Whitehead P (2006) The measurement of residual stresses by the incremental hole drilling technique. *Measurement Good Practice Guide No. 53 - Issue 2: 63*
- Oettel R (2000) The determination of uncertainties in residual stress measurement (using the hole drilling technique). *Standards Measurement & Testing Project No. SMT4-CT97-2165 - Issue 1: 18*
- (2010) Micro Measurements. Special use sensors - residual stress strain gages <http://www.vishaypg.com/docs/11516/resstr.pdf>. Accessed 5 Apr 2016
- Kirsch G (1898) Theory of elasticity and application in strength of materials. *Zeitschrift Vevein Dtsch Ingenieure* 42:797–807
- (2014) Micro Measurements. Instruction bulletin B-129-8: Surface preparation for strain gage bonding <http://www.vishaypg.com/docs/11129/11129B129.pdf>. Accessed 5 Apr 2016
- (2011) Micro Measurements. Milling guide for residual stress measurements <http://www.vishaypg.com/docs/11304/rs200.pdf>. Accessed 5 Apr 2016
- Nau A, Feldmann GG, Nobre JP et al (2014) An almost user-independent evaluation formalism to determine arbitrary residual stress depth distributions with the hole-drilling method. In: Kurz SJB, Mittemeijer EJ, Scholtes B (eds) International conference on residual stresses 9. Trans Tech Publications, Garmisch-Partenkirchen, p 778
- Schajer GS. H-Drill – hole-drilling residual stress calculation program. Vancouver, Canada. <http://www.schajer.org/>
- Zuccarello B (1999) Optimal calculation steps for the evaluation of residual stress by the incremental hole-drilling method. *Exp Mech* 39:117–124
- Casavola C, Pappaletta G, Pappaletta C et al (2013) Analysis of the effects of strain measurement errors on residual stresses measured by incremental hole-drilling method. *J Strain Anal Eng Des* 48:313–320